

# POWER ABSORPTION DURING NONLINEAR ELECTRON CYCLOTRON WAVE-PARTICLE INTERACTION \*

R. Kamendje<sup>1</sup>, S. Kasilov<sup>2</sup>, W. Kernbichler<sup>1</sup>, M.F. Heyn<sup>1</sup>

<sup>1</sup>Institut für Theoretische Physik, Technische Universität Graz  
Petersgasse 16, A-8010 Graz, Austria

<sup>2</sup>Institute of Plasma Physics

National Science Center “Kharkov Institute of Physics and Technology”  
Ul. Akademicheskaya 1, 61108 Kharkov, Ukraine

## 1. Introduction

The linear theory of wave absorption and the quasilinear theory of the evolution of the distribution function are presently the main tools for a quantitative description of ECRH and ECCD in fusion devices. However, the applicability of these theories is violated for some ECRH (ECCD) scenarii in typical experimental conditions. In particular, this is true for one of the basic scenarii where the 2<sup>nd</sup> harmonic electron cyclotron resonance for the extraordinary mode (X-mode) is used. Formally, the quasilinear description of wave-particle interaction remains valid if the particle flight time through the radiation beam,  $t_f$ , is small compared to the oscillation period of a particle trapped in the wave,  $\tau_{bE}$ . This condition is satisfied only for particles with relatively large parallel velocities as compared to the perpendicular velocity. On the other hand, in the opposite limit case,  $t_f \gg \tau_{bE}$ , whenever typical experimental conditions are considered, the adiabatic theory (see, e.g., Ref. [1]) which is only applicable in the region of phase space with small parallel velocities does not give correct quantitative results for both the particle distribution function and the absorbed power as long as calculations of these quantities are done without taking into account the combined effect of wave-particle interactions and collisional processes.

Since the domain of phase space where the nonlinearity parameter  $\epsilon_{NL} = t_f/\tau_{bE}$  is of the order of one and which is neither covered by the (quasi)linear nor by the adiabatic approximation occupies a significant part of this space, the problem of wave-particle interaction has to be treated numerically.

## 2. Formulation of the problem

During ECCD (ECRH), the electron distribution function is determined by resonant wave-particle interaction processes which take place in the small power deposition region as well as by the effects of particle drift motion and Coulomb collisions in the main plasma volume. In the present study, the main interest is in the development of a proper model of wave-particle interaction, which in turn can be used for particular cases of magnetic field geometry. The influence of the device geometry in its full extent can be handled by the stochastic mapping technique [2,3] (SMT) where the modelling of stochastic processes is separated from the modelling of drift orbits which are pre-computed and used in the form of Poincaré maps. As in SMT, also in the present report, a formulation of equations in terms of the conservation of the particle

---

\*This work has been carried out within the Association EURATOM-ÖAW and under contract P13495-TPH with the Austrian Science Foundation as well as with funding from the Friedrich Schiedel Stiftung für Energietechnik.

flux density through Poincaré cuts in phase space is used (see Ref. [4]). Instead of recalculation of particle orbits each time a particle passes through the wave beam, these orbits are pre-computed and used for the construction of a transition probability density which fully describes the orbit change by the wave particle interaction if the wave-particle phase is random when the particle enters the beam. In the present report, a simplified geometry is assumed which should qualitatively represent typical experimental conditions. Within this model, the uniform main magnetic field is directed along the  $Z$ -axis and a narrow Gaussian radiation beam propagates across the main magnetic field in the  $XZ$ -plane. The system is periodic in the  $Z$ -direction with the period  $L$ . Such a simple model geometry is representative, e.g., for the magnetic axis of a tokamak.

The particle motion in the wave electric field  $\mathbf{E} = E_0 \text{Re} [\mathbf{f} \exp(-z^2/(2L_b^2) + i(k_\perp x + k_\parallel z - \omega t))]$  is described by the Hamiltonian  $\hat{H} = \Omega w - w^2/2 + \varepsilon w e^{-\tau^2} \cos \psi$  where

$$\Omega = \frac{\sqrt{2}L_b}{|v_\parallel|} \left( k_\parallel v_\parallel - n_0 \omega_{c0} \left( 1 - \frac{v_\parallel^2}{2c^2} \right) - \omega \right), \quad \varepsilon = \frac{\sqrt{2}L_b |f^-| v_E k_\perp}{|v_\parallel|}.$$

Here,  $E_0 = \text{const}$  and  $\mathbf{f} \equiv \mathbf{E}/|\mathbf{E}| = \text{const}$  are the wave amplitude and the polarization vector, respectively,  $\tau = |v_\parallel|t/(\sqrt{2}L_b)$ ,  $w$ ,  $\psi$ ,  $L_b$ ,  $\omega$ ,  $c$  are the dimensionless time, the dimensionless particle perpendicular energy, the wave-particle phase, the beam width, the wave frequency and the speed of light, respectively. Further,  $v_E \equiv eE_0/(m_0\omega)$ ,  $m_0$  is the particle mass,  $\omega_{c0}$  is the gyrofrequency at rest and  $e$  is the electron charge.

Introducing at the sides of the beam cuts A and B at positions  $z = -\delta L/2$  and  $z = \delta L/2$ , respectively, where  $L_b \ll \delta L \ll L$ , the kinetic equation is reduced to a set of integral relations between the pseudo-scalar particle flux densities through the neighboring cuts,  $\Gamma = |v_\parallel|Jf$ . Here  $J = v_\perp$  and  $f$  are the phase space Jacobian and the distribution function, respectively. Combined together using the periodicity of the problem, the relations which map the flux through the wave beam and through the outer region form an integral equation (see Ref. [4]), which is then solved using a Monte Carlo method.

### 3. Results of the modelling

The level contours of the nonlinearity parameter  $\epsilon_{NL} = L_b |\omega_{c0}| v_\perp / (c |v_\parallel|) \sqrt{E_0 N / B_0} \sim \sqrt{\Omega \varepsilon} \sim P_b^{1/4} B_0^{1/2} L_b^{1/2} \tan \chi$  ( $\tan \chi = v_\perp / v_\parallel$ ) are plotted in Fig. 1 for two values of the power in the beam,  $P_b = 400$  kW (red lines) and  $P_b = 100$  kW (blue lines),  $B_0 = 2.55$  T and  $L_b = 2$  cm. This picture reveals that, for parameters relevant for present day experiments, there is a wide region in velocity space where none of the limit cases of electron cyclotron wave-particle interaction is valid. Note that the depicted levels are only slightly modified when changing the power. Therefore, the change of the power within the range of present day experimental values does not make either of the limiting cases fully applicable. For the points labeled A, C and D around the resonance line  $\omega = 2|\omega_c|$  in Fig. 1, within the resonance zone in velocity space, Fig. 3 shows the dependence of the normalized particle perpendicular energy after one pass through the wave beam,  $W_N$ , versus the initial wave-particle phase,  $\psi$ , for the beam power  $P_b = 400$  kW. With increasing  $\epsilon_{NL}$  (from point A to point D),  $W_N(\psi)$  moves away from the nearly harmonic behavior which is characteristic for the (quasi)linear interaction regime to the nonlinear one.

In Fig. 2 a typical particle distribution in the nonlinear case is shown for Cut A for zero

(left) and finite  $N_{\parallel} = ck_{\parallel}/\omega$  (right) values. Even for  $N_{\parallel} = 0$ , the distribution function is asymmetric and a plateau-like structure is formed around the resonance zone.

The field line integrated absorbed power density,  $\overline{P_{abs}} \equiv \int dz P_{abs}$ , corresponds to the difference between the incoming energy flux density on Cut A (B) and the outgoing energy flux density on Cut B (A),

$$\overline{P_{abs}} = 2\pi \int_0^{\infty} dv_{\perp} \int_{-\infty}^{\infty} dv_{\parallel} \left( \Gamma_B(v_{\perp}, v_{\parallel}) - \Gamma_A(v_{\perp}, v_{\parallel}) \right) \frac{mv^2}{2} \text{sign} v_{\parallel}. \quad (1)$$

Integrating the energy conservation law,  $\nabla \cdot \mathbf{S} + P_{abs} = 0$ , with  $\mathbf{S}$  being the Poynting flux, along the magnetic field line, a nonlinear differential equation for the wave amplitude is obtained,

$$\overline{P_{abs}} = -\frac{\partial}{\partial x} \overline{S_x}, \quad \overline{S_x} \equiv \int dz S_x = \frac{cL_b}{8\sqrt{\pi}} \left[ (|f_y|^2 + |f_z|^2) N_{\perp} - |f_x||f_z|N_{\parallel} \right] E_0^2(x). \quad (2)$$

Here  $f_x$ ,  $f_y$  and  $f_z$  are components of the polarization vector,  $N_{\parallel}$  and  $N_{\perp}$  are the parallel and the perpendicular components of the refractive index, respectively. Here, the model assumption is used that the beam shape is not changed by the absorption. For the computation of radial profiles the magnetic field dependence on  $x = R - R_0$  of the form  $B = B_0 R_0 / R$  has been assumed where  $R_0 = 200$  cm.

In order to study the reduction of the absorbed power density  $\overline{P_{abs}}$  and, respectively, of the absorption coefficient  $\alpha = \overline{P_{abs}}/\overline{S_x}$  as compared to the results of the linear theory, besides the nonlinear model of this paper and the quasilinear model, the following models have been used in Fig. 4. The first two models correspond to the often used assumption that the distribution of electrons which enter the wave beam is a Maxwellian. The respective curves in Fig. 4 are denoted as “(Maxwell)” in the legends. In some extent, this assumption models the exact particle dynamics in the outer region in case of a short mean free path regime. In addition, the adiabatic model has been examined within the present approach. The corresponding curves are labeled with “adiabatic” in the legends. The linear absorption coefficient has been obtained using the fully relativistic computation of Refs. [5] modified here for the finite plasma density case.

As one could expect, the absorption coefficients obtained using a Maxwellian only weakly depend on plasma density through such a dependence of the polarization vector  $|f^-|$  and the refractive index  $N_{\perp}$ . The reduction of this coefficient is purely due to nonlinear effects which limit the maximum change in perpendicular velocity of electrons to the width of the resonance zone  $\Delta v_{\perp} \sim (cv_E)^{1/2}$ . With changing power from 400 kW to 4 kW, the “adiabatic Maxwellian” absorption coefficient increases approximately 3 times. In order to analyze these dependencies, it is sufficient to study the case when both, the linear width of the resonance zone over the perpendicular velocity which is due to the finite beam width,  $L_b$ , and the nonlinear width are much smaller than the value of the perpendicular velocity on the resonance line,  $v_{\perp r}$ . The ratio of the “adiabatic Maxwellian” absorption coefficient,  $\alpha_A$ , to the linear coefficient,  $\alpha_L$ ,  $\alpha_A/\alpha_L = \left( 2^{11/2} c^{3/2} \right) / \left( \pi^{9/2} \omega L_b (v_E |f^-| N_{\perp})^{1/2} \right)$ , scales with power as  $P^{-1/4}$  which explains the increase in the “adiabatic Maxwellian” absorption coefficient  $\sqrt{10} \approx 3$  times with decreasing power. At the same time, the absorption coefficient computed within the approach of the present paper for a Maxwellian distribution does not follow this simple scaling because the adiabatic theory is never applicable in velocity space as a whole.

The effects of the nonlinear (quasilinear) plateau formation appear to have much stronger

influence on the absorption coefficient in the cases considered here. The reduction of the nonlinear absorption coefficient in the high power case ( $P = 400$  kW) as compared to the linear coefficient is 44, 18, and 5.6 times for the density values  $10^{13}$  cm $^{-3}$ ,  $3 \cdot 10^{13}$  cm $^{-3}$ , and  $10^{14}$  cm $^{-3}$ , respectively. (The absorption coefficients are compared at  $R = 197$  cm which corresponds to the maximum of the linear absorption coefficient.) Roughly, the nonlinear absorption coefficient scales with density, i.e. it is proportional to the collisionality. The results with a non-Maxwellian distribution function obtained using the quasilinear or the adiabatic model have approximately the same scaling. In cases considered here, they give values of the same order, as compared to the nonlinear case presented in this report. At the same time, the discrepancy can be observed at the highest density which corresponds to the shortest mean free path regime. In this case, the quasilinear model underestimates the power absorption. It should be noted that “long mean free path” regimes here are not the same as in the neoclassical transport theory because the mean free path should be compared to the length which is needed by the field line to re-enter the wave beam. This length can be much longer than the tokamak connection length in the case of off-axis heating.

Combining the results of Eq. (1) and Eq. (2) allows for a self-consistent computation of the radial profiles of the wave amplitude,  $E_0$ , of the absorbed power density,  $\overline{P_{abs}}$ , of the nonlinear absorption coefficient,  $\alpha_{NL}$ , and of the optical thickness,  $\tau = \frac{1}{2} \int_0^x \alpha_{NL}(x') dx'$ , as presented in Figures 5 and 6 together with the predictions of the linear and the quasilinear approximations. As a result of the reduction of the absorption coefficient, a broadening of the absorption profile occurs which is more pronounced for lower plasma densities. As a consequence, for the density value  $n_e = 3 \cdot 10^{13}$  cm $^{-3}$  the radiation “shine through” occurs in the case where the linear theory predicts the complete wave absorption (optical depth  $\tau = 22.5$ , see Fig. 6). It should be noted that, in this particular case, the nonlinear and the quasilinear model give similar results despite the different picture of power deposition in the velocity space. This coincidence, however, need not to be always the case (see Fig. 4).

Using the distribution function shown in Fig. 2, the distribution of the current density in velocity space (Fig. 7 left),  $e(\Gamma(v_{||}) - \Gamma(-v_{||}))$  is computed. The result shows that the current is generated mainly by particles above the resonance line (black line in Fig. 2 and 7). Moreover, the current density distribution over the pitch angle  $\chi$  (Fig. 7 right) indicates that the highest current is produced by particles with pitch angles larger than  $45^\circ$ . Those particles interact with the wave in the nonlinear regime.

#### 4. Conclusions

A numerical model for ECRH and ECCD which consistently takes into account nonlinear wave-particle interaction has been developed. The results of computations show that the distortion of the particle distribution function from Maxwellian is strong for parameters typical for present day ECRH experiments. This leads to a reduction of the absorption, consequent broadening of the absorption profile and incomplete absorption. It should be mentioned that the distortion of the particle distribution function is essentially different from what is expected from the quasilinear theory where a Fokker-Planck equation is assumed to be valid. The positive derivative of the distribution function indicates that nonlinear effects of ECRH may cause the electron Bernstein wave instability.

The modelling of ECCD at the 2<sup>nd</sup> harmonic X-mode resonance shows that the effect of power redistribution in velocity space can especially be important for current drive. Therefore, for ECCD the absorption should be taken into account correctly by using

nonlinear computations. It should be mentioned that the noise in the right picture in Fig. 7 due to poor statistics in the tail of the distribution function where the main part of the current is generated can be resolved using the weight-windows algorithm [6], that will be realized in future computations.

With increasing both magnetic field and size of the beam, the nonlinear effects become more important ( $\epsilon_{NL}$  is increasing). Therefore, the proper account of nonlinear effects is ultimate for reactor-scale devices.

## References

- [1] I.A. Kotel'nikov and G.V. Stupakov, *Phys. Fluids B*, **2**, 881 (1990).
- [2] S.V. Kasilov, E. Moiseenko, and M.F. Heyn. *Physics of Plasmas*, **7**, 2422 (1997).
- [3] S.V. Kasilov, W. Kernbichler, V.V. Nemov and M.F. Heyn. *Physics of Plasmas*, **9**, (August 2002).
- [4] R. Kamendje, S.V. Kasilov, W. Kernbichler and M.F. Heyn, in *28th EPS Conf. on Contr. Fusion and Plasma Physics*, **25A**, Madeira, Portugal, The European Physical Society, Petit-Lancy, 817 (2001).
- [5] S.V. Kasilov and W. Kernbichler. *Physics of Plasmas*, **3**, 4115 (1996).
- [6] S.V. Kasilov, E. Moiseenko, M.F. Heyn and W. Kernbichler, in *12<sup>th</sup> Topical Conference on Radio Frequency Power in Plasmas, Savannah, Georgia, 1997. AIP Conference Proceedings* (American Phys. Soc., New York, 1997), **403**, 321.

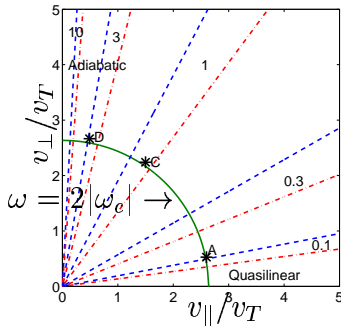


Figure 1: Domains of validity of the different models, dashed and dashed-dotted lines correspond to the values of the power in the beam  $P_b = 400$  kW and  $P_b = 100$  kW , respectively.

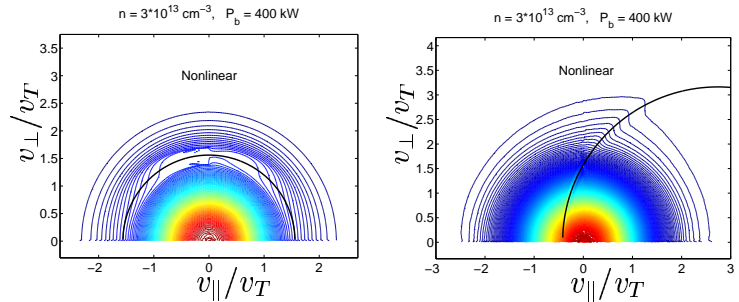


Figure 2: Distribution function at cut A for the case  $N_{\parallel} = 0$  (left) and  $N_{\parallel} = 0,3$  (right).

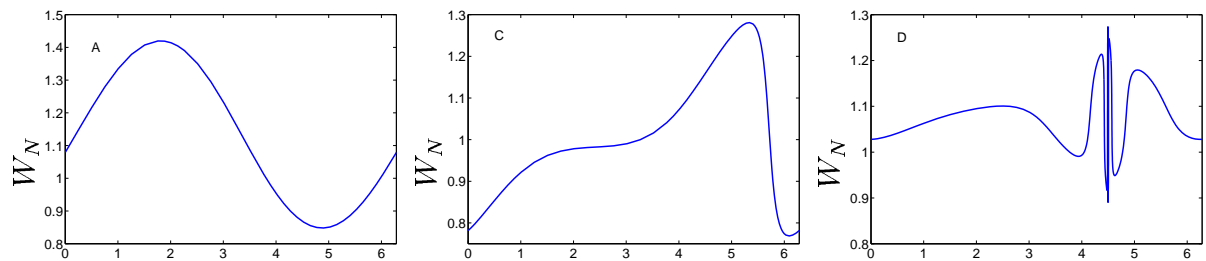


Figure 3: Normalized particle perpendicular energy after traveling through the wave beam  $W_N$  versus initial wave-particle phase  $\psi$ ,  $N_{\parallel} = 0$ . The Labels A, C, and D indicate that the respective curve is plotted for its pertinent starting point in velocity space marked in Fig. 1. The corresponding pitch angle values are  $\chi = 11.47^\circ$ ,  $56.2^\circ$  and  $79.6^\circ$ , respectively.

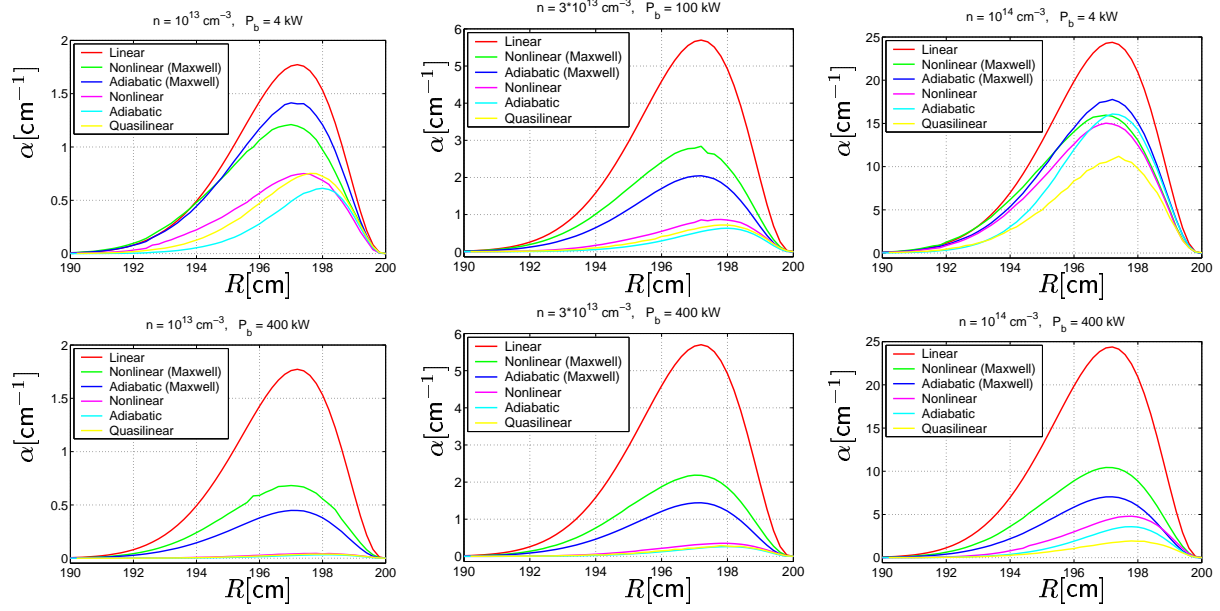


Figure 4: Profiles of the absorption coefficient  $\alpha$  along the major plasma radius  $R$  for different input power values, different plasma densities, constant amplitude of the wave electric field along  $R$  and  $N_{\parallel} = 0$ .

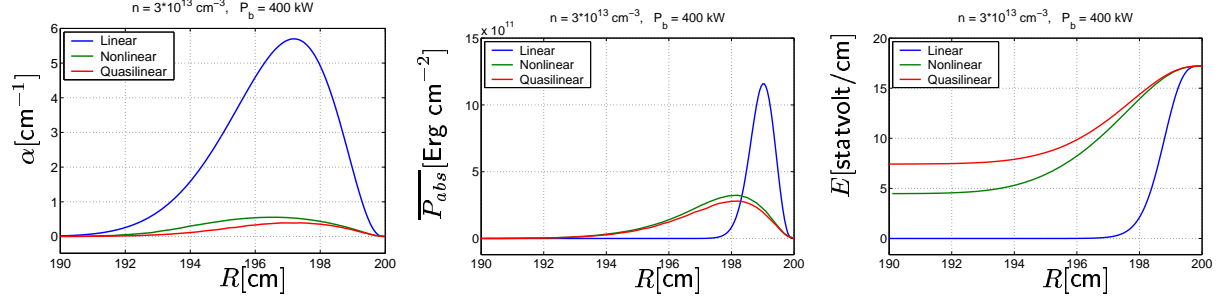


Figure 5: Radial profiles of the self-consistently computed absorption coefficient  $\alpha$ , field line integrated absorbed power density  $\overline{P_{abs}}$  and electric field amplitude  $E$  compared with those of the linear and the quasilinear approximation.  $N_{\parallel} = 0$ .

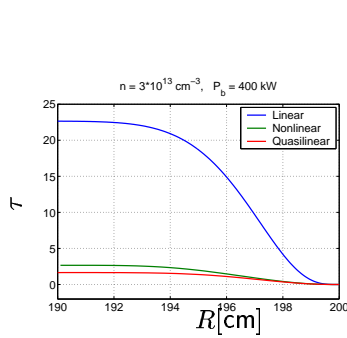


Figure 6: Radial profile of the self-consistently computed optical thickness  $\tau$  compared with those of the linear and the quasilinear approximation.  $N_{\parallel} = 0$ .

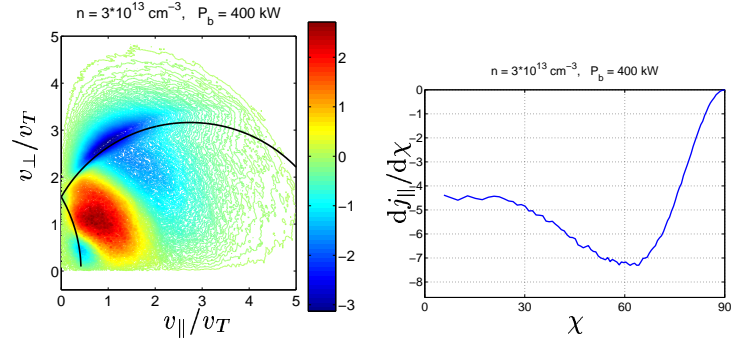


Figure 7: Distribution in velocity space of the parallel current density (left) and distribution of the same quantity over the pitch angle (right) (Here  $N_{\parallel} = 0.3$ ).